AIAA 95-6093
Low-Speed Wind Tunnel Tests of Two Waverider Configuration Models

Robert J. Pegg
David E. Hahne
Charles E. Cockrell, Jr.
NASA Langley Research Center
Hampton, VA 23681-0001

Sixth International Aerospace Planes and Hypersonics Technologies Conference
April 3-7, 1995 / Chattanooga, Tennessee

LOW-SPEED WIND TUNNEL TESTS OF TWO WAVERIDER CONFIGURATION MODELS

Robert J. Pegg,* David E. Hahne,† and Charles E. Cockrell, Jr.‡
NASA Langley Research Center
Hampton, VA 23681-0001

Abstract

A definitive measurement of the low-speed flight characteristics of waverider-based aircraft is required to augment the overall design database for this important class of vehicles which have great potential for efficient high-speed flight. Two separate waverider-derived vehicles were tested; one in the 14- by 22-Foot Tunnel and the other in the 12-Foot Low-Speed Tunnel at Langley Research Center. These tests provided measurements of moments and forces about all three axes, control effectiveness, flow field characteristics and the effects of configuration changes. This paper will summarize the results of these tunnel tests and show the subsonic aerodynamic characteristics of the two configurations.

Introduction

Technologies related to high speed flight (the Mach 4 to 6 speed range) have matured in the last ten years to a level where serious consideration of a vehicle incorporating these technologies is warranted. A high speed vehicle could perform missions such as: cruise missile carrier, high altitude reconnaissance platform, long range strike aircraft, and long range transport. Aircraft derived from shapes based on the waverider theory offer one approach to providing the designer with a configuration which shows great potential when used for the previously listed missions. A long range design effort using this type of configuration was made and is reported in Ref. 1.

Numerous studies (Refs. 2, 3, and 4) have been made which detail the concept of the superiority of the waverider shape in achieving high L/D at a design flight point. The waverider shape also offers potential advantages in propulsion/airframe integration for airbreathing hypersonic vehicles (Ref. 5). The aerodynamic attractiveness of this type of configuration has generated much interest with aircraft designers. Practical design considerations, however, require that a waverider-derived aircraft have a cockpit, engines, and other drag producing necessities. Aftbody closure is also a significant challenge due to the thick bases present on waverider shapes. The research presented in this paper was initiated as part of an on-going NASA conceptual design study to develop a data base for use in the analysis and design of hypersonic vehicles. Because studies have shown that the aerodynamic and stability and control characteristics of proposed hypersonic aircraft during take-off, initial climb, and approach phases of flight will greatly influence the ultimate vehicle design, an experimental investigation of two different waverider-based configurations showing the effects of protuberances on the performance at low speeds (up to dynamic pressures of 90 psf) were made.

Symbols

Longitudinal forces and moments are presented in the stability-axis system. Lateral-directional forces and moments are presented in the body-axis system.

b	wing span, ft
C_D	drag coefficient
C_L	lift coefficient
C_ι	rolling-moment coefficient
$C_{\iota\beta}$	rolling-moment derivative, $\partial C_\ell / \partial \beta$
C_m	pitching-moment coefficient
C_n	yawing-moment coefficient
$C_{n\beta}$	Yawing moment derivative, $\partial C_n / \partial \beta$
C_Y	side-force coefficient
L/D	lift to drag ratio

* Asst. Manager, Systems Analysis Office, HVO.
† Aerospace Engineer, Vehicle Dynamics Branch, Flight Dynamics and Control Division.
‡ Aerospace Engineer, Hypersonic Airbreathing Propulsion Branch, Gas Dynamics Division, Member, AIAA.

l	body length, ft
q	free-stream dynamic pressure, lbf/ft^2
S	wing-body planform area, ft^2
V	freestream velocity, kts
W	vehicle weight, lbf
X, Y, Z	body axes
α	angle of attack, deg.
β	angle of sideslip, deg.
ΔC_l	incremental rolling-moment coefficient
ΔC_n	incremental yawing-moment coefficient
ΔC_Y	incremental side-force coefficient
δ_t	tiperon deflection, positive trailing-edge down, deg
δ_r	rudder deflection, positive trailing-edge left, deg
δ_A	aileron deflection angle, deg.
δ_E	elevon deflection angle, deg.

Subscripts:

o	value at zero angle of attack
trim	trimmed value (Cm = 0)

Abbreviations:

BW	body with blended wing
N	engine nacelle
V	vertical tails

Model Descriptions

A photograph of the Mach 4.0 waverider-derived hypersonic cruise configuration is shown in Fig. 1 and a 3-view drawing is shown in Fig. 2. The design of this configuration allows for removal and testing of two different leading edge shapes, creating two distinct configurations. These configurations are referred to as the straight-wing and cranked-wing models. The straight-wing model is shown in the photograph in Fig. 1, while the cranked-wing tips are shown as a separate model part in this figure. These wing surfaces replace the straight-wing tips to create the cranked-wing vehicle. The term "cranked" in this case refers to a shape where the sweep angle not only changes, but also where the leading edge curves upward to add a significant amount of dihedral in the aft portion of the wing. The cranked-wing shape was designed to provide improvements in subsonic aerodynamic performance due to a small increase in aspect ratio as well as improvements in lateral-directional stability over the straight-wing design. The pure waverider forebodies (both the straight and cranked waveriders) are conical-flow-derived waveriders and were optimized for maximum lift-to-drag ratios at Mach 4.0 using the method developed by Bowcutt (Ref. 3) and modified by Corda (Ref. 6), at the University of Maryland. Both waverider forefodies were developed from the same conical flow field. The waverider forebodies were integrated into realistic waverider-derived hypersonic cruise configurations. A faceted canopy, representative of a hypersonic cruise vehicle canopy, was designed and fabricated for the model as well as a propulsion system, which consisted of an inlet compression ramp, a non-flow-through engine module with two side walls and a nozzle/expansion surface. A smooth canopy was also fabricated and may be substituted for the faceted canopy in order to isolate the canopy effect on aerodynamic performance. Control surfaces for each of these configurations consisted of elevons and ailerons at fixed deflection angles of 0°, positive 20° (trailing-edge down) and negative 20° (trailing-edge up) as well as a fixed vertical tail. The moment reference center used here is at a location equal to 62.5 percent of the centerline chord length of the vehicle. Details of the model design are included in Refs. 7 and 8. These configurations have been tested previously at Mach numbers from 1.6 to 4.63 and the results were also reported in Refs. 7 and 8.

The second model tested (shown in Fig. 3) is a .062-scale model of a waverider-derived hypersonic vehicle study concept (Ref. 1) which was optimized for a Mach 5 flight condition and is referred to as LoFlyte. The configuration consists of a blended wing-body, twin wing-mounted vertical tails, and an engine nacelle package located on the underside of the body. The engine nacelle was a simple flow-through shell attached to the underside of the body. A three-view drawing with dimensions is shown in Fig. 4. Each vertical tail had a notch cut out of the rudder nearest the wing to prevent physical interference with the tiperons; an alternate vertical tail was tested with this notch filled. The moment reference center is located at 58 percent of the body length for this configuration

Tests

The two Mach 4.0 hypersonic cruise configurations were tested in the NASA-Langley 14x22-foot subsonic wind tunnel while the 0.062-scale LoFlyte model was tested in the NASA-Langley 12-foot low-speed tunnel. A description of the 14x22-foot tunnel is contained in Ref. 9. A detailed list of data entries for both experiments is presented in Tables 1 and 2.

The Mach 4.0 model was tested at dynamic pressures ranging from 30 to 90 psf, with most runs at 90 psf (Mach number of approximately 0.25). Unless otherwise indicated, all data shown in this paper for these configurations were obtained at the 90 psf condition. Data obtained consisted of 6-component force and moment data obtained over an angle of attack range of -6° to 20° at sideslip angles of 0°, 3°, and 6°. Flow visualization data was also obtained from a smoke stream and laser light-sheet to supplement the force and moment data. Model 2 data were obtained at a dynamic pressure of 4 psf. This corresponds to a Reynolds number of 3.08×10^6 based on body length. Force and moment coefficients were obtained over an angle-of-attack range between -5° and 22° at sideslip angles of 0°, -4° and 4°. Limited laser light-sheet flow visualization studies were also conducted to help interpret the force and moment data.

Results And Discussion

Model 1

Results from experimental tests of the Mach 4.0 hypersonic cruise configurations are presented by showing a comparison of the aerodynamic characteristics of the straight-wing and cranked-wing fully-integrated vehicles followed by an analysis of the control surface effectiveness. Unless otherwise stated, the configurations are assumed to have the realistic faceted canopy, the propulsion system components, 0° ailerons, 0° elevons and the vertical tail attached. The control surface effectiveness discussion will focus primarily on the straight-wing vehicle. This discussion will show the pitch control effectiveness of the ailerons and elevons, roll control effectiveness of the ailerons and a combined aileron/elevon deflection and finally, the effects of combined roll/pitch control.

The aerodynamic performance characteristics of the straight-wing and cranked-wing Mach 4.0 waverider-derived hypersonic cruise configurations are summarized in Figs. 5–7. Data presented for the cranked-wing configuration were taken at a dynamic pressure of 85 psf due to difficulties maintaining tunnel flow at the 90 psf condition. In each case, the coefficient data were reduced by the individual planform areas of each configuration. No attempt was made in the data analysis to correct for drag of the propulsion nacelles surfaces. Therefore, the data shown include both aerodynamic and propulsive drag forces and are representative of the performance of an unpowered configuration. Figure 5 shows a comparison of lift coefficient values for the two configurations. The cranked-wing vehicle shows slightly higher lift coefficient values than the straight-wing vehicle at angles of attack below 16°. This difference is diminished at higher angles of attack. The shape of the lift curve is non-linear, with the slope of the lift curve increasing as angle of attack increases. The strong vortex flows present, which were observed in flow visualization data, are primarily responsible for these non-linear aerodynamic characteristics. Figure 6 shows that there are no significant differences in drag values between the two configurations. The lift-to-drag ratios for each configuration are shown in Fig. 7. The cranked-wing model has slightly higher lift-to-drag ratios than the straight-wing model at positive angles of attack between 0° and 8°. At higher angles of attack, there is no significant difference between the two configurations. The maximum lift-to-drag ratios observed experimentally are approximately 5.8 for the cranked-wing model and approximately 5.4 for the straight-wing model. Based on these results, the cranked-wing design offers only a marginal advantage in subsonic aerodynamic performance compared to the straight-wing design.

The static longitudinal stability of each of the two configurations is shown in Fig. 8. The pitching moment curve is non-linear due to the influence of vortex-dominated flows. At the 90 psf dynamic pressure condition, the aerodynamic center of the straight-wing vehicle is estimated to be at a location equal to approximately 50 percent of the centerline chord. Therefore, the center of gravity must be placed ahead of this location in order to achieve longitudinal stability. Similar problems with the longitudinal stability of waveriders and waverider-derived configurations were noted in Refs. 10 and 11.

The lateral-directional stability characteristics of the straight-wing and cranked-wing vehicles are shown in Figs. 9 and 10. Figure 9 shows yawing moment derivatives, $C_{n\beta}$, for each configuration while Fig. 10 shows rolling moment derivatives, $C_{\iota\beta}$. The stability derivatives were calculated using angle of attack sweeps at 0° and 6° sideslip angles, assuming a linear relationship between the moment coefficients and the sideslip angle. The cranked-wing configuration shows better lateral-directional stability than the straight-wing vehicle due to the increased dihedral from the cranked wings. Both configurations are stable with respect to roll and yaw, except that the straight-wing configuration

shows a roll instability at negative angles of attack at these freestream conditions. The effect of the fixed vertical tail on the directional stability of the straight-wing model is shown in Fig. 11. The results show that the addition of the vertical tail contributes significantly to directional stability and also the body itself produces high levels of directional stability at the higher angles of attack. This phenomena will be discussed further in relation to models. A similar effect is observed for the cranked-wing configuration. No rudder deflection runs were done for these configurations.

The pitch control effectiveness of the ailerons and elevons for the Mach 4.0 straight-wing waverider-derived hypersonic cruise vehicle is shown in Figs. 12 and 13. Figure 12 shows lift coefficient values and Fig. 13 shows pitching moment coefficient values for elevon deflection angles (δ_E) of 0° as well as positive (trailing-edge down) and negative 20°. Data are also shown for a combined elevon and aileron deflection angle (δ_A) of positive 20°. The elevons are less effective in pitch control than the ailerons at angles of attack below 8°, as evidenced by the smaller increments in lift and pitching moment observed for the elevon-only deflections. At higher angles of attack, the elevons become more effective than the ailerons. In order to turn this configuration at representative take off and landing angles of attack, either more pitch control or CG movement is necessary.

The roll control effectiveness of the ailerons and a combined aileron/elevon deflection for the straight-wing vehicle are shown in Figs. 14 and 15. Figure 14 shows rolling moment increments produced by an asymmetric aileron deflection of positive 20° on one side and negative 20° on the opposite side. The elevons are fixed at 0° for this case. Also shown are the increments produced by a combined asymmetric elevon and aileron deflection. The rolling moment increments produced by the aileron and aileron/elevon deflections are constant from approximately -2° to 7° angle of attack and then decrease as angle of attack decreases. Yawing moment increments for the same deflection angles are shown in Fig. 15. The amount of yaw moment produced by the aileron and aileron/elevon deflections is small, but does become adverse above angles of attack above 6°–8°.

The effectiveness of combined roll and pitch control for a 20° asymmetric aileron deflection and a positive 20° symmetric elevon deflection is shown in Figs. 16 and 17. Figure 16 shows rolling moment increments produced for the combined roll/pitch deflection compared to an asymmetric aileron deflection alone. The effectiveness of the aileron deflections are reduced when combined with a symmetric elevon deflection. Figure 17 shows pitching moment coefficients produced by a 20° symmetric elevon deflection in combination with a 20° asymmetric aileron deflection and for the elevon deflection alone. There is no significant difference between these two cases, indicating that the addition of an aileron deflection does not inhibit the pitch control effectiveness of the elevons at these operating conditions.

Most of the control surface effects observed for the cranked-wing configuration are not significantly different from those observed for the straight-wing vehicle. However, one significant difference is that the cranked-wing ailerons produce significantly less rolling moment increments for a 20° asymmetric aileron deflection than the straight-wing ailerons at angles of attack above 1°. Additionally, the cranked-wing ailerons produce significantly more adverse yaw than the straight wing at similar conditions.

Model 2

Longitudinal Characteristics - The effect of the configuration components on the longitudinal characteristics of the model are shown in Fig. 18. These components include the engine nacelle (N) and the vertical tails (V). For the body-wing and the body-wing-nacelle configurations, the influence of a strong leading-edge vortex can be seen in both the lift and pitching moment coefficients. In lift, this influence can be seen as a constant increase in the lift curve slope above $\alpha = 4°$. The effect on pitching moment is seen as a mild pitch-up that begins near the same angle of attack. The lift and pitching moment data in this figure show that the vertical tails interact with the leading-edge vortex system. This is evidenced by the decrease in the lift curve slope seen for the tail-on configurations at angles of attack above 8° and by small but distinct changes in pitch stability at $\alpha = 11°$ and 15°. Flow visualization data also showed that the path of the leading-edge vortex was very close to the baseline vertical tail location. While the decrease in lift curve slope was expected the behavior in pitch was not typical for wing-mounted vertical tails on this type of configuration. Normally, wing-mounted vertical tails will cause the leading-edge vortex to burst prematurely resulting in a pitch-up. However,

the addition of the vertical tails results in an increase in pitch stability before the unstable pitch-up for this configuration. The reason for this behavior is not currently understood.

The effectiveness of the tiperons for providing pitch control is presented in Fig. 19. The tiperons were sized to provide enough pitch control to trim the vehicle up to 16° angle of attack with no more than 10° of surface deflection. This was confirmed by the data, which show that about a 10° tiperon deflection is indeed sufficient to trim the configuration up to the desired angle of attack of 16°. Tiperon effectiveness drops off for deflections above 10°, however, and this may be a concern in generating sufficient nose-down pitch rates for recovery from angles of attack above 15°. An analysis using representative weights and inertias for this type of vehicle (using approach-to-landing conditions) was therefore made to determine the nose-down pitch control requirements. This analysis used the criteria discussed in Refs. 12 and 13 for relaxed pitch stability configurations to determine the required level of nose-down pitching moment for satisfactory recovery response. The results indicate that the present configuration would have satisfactory recovery characteristics.

Figure 20 shows the results of calculations to determine the trimmed values of C_L and L/D as well as the tiperon deflection required for trim. Drag values include the effect of the engine nacelle. Because of the pitching moment characteristics of this configuration (neutral to unstable static margin and positive $C_{m,o}$) the vehicle has a reasonably high level of unpowered trimmed C_L at nominal takeoff and approach-to-landing conditions ($\alpha = 10°$). As a result takeoff speeds at full gross weight (551,052 lbs) of 263 kts are possible. If the lift component of thrust and the expected nose-up pitching moment due to thrust were to be accounted for then the takeoff speed would be significantly less than 263 kts. For approach-to-landing conditions the approach speed for a nominal weight of 183,000 lbs would be 151 kts. While high as compared to most conventional aircraft, this is judged to be a reasonable speed for this class of vehicle (shuttle orbiter landing speeds are in excess of 200 kts).

Lateral-Directional Characteristics - The effect of the configuration components on lateral-directional characteristics are presented in Fig. 21. As would be expected for a configuration with such a highly swept planform, the level of lateral stability increases with angle of attack. The high levels of lateral stability observed, however, may have an adverse impact on landing operations in crosswind conditions. At the higher angles of attack, the vertical tails tended to reduce lateral stability. Flow visualization studies indicated that at these angles of attack, the windward leading-edge vortex is very close to the outboard side of the windward vertical tail. In fact, flow from the leading-edge vortex actually causes a small vortex to form on the vertical tail. These two regions of low pressure acting on the windward face of a surface above the center of gravity of the configuration would tend to reduce lateral stability.

Without the vertical tails, the configuration, as expected, was unstable directionally up to 11° angle of attack. Above these angles of attack the wing-body configuration exhibits stable values of Cn_β that appear to be due to forces aft of the center of gravity (C_{Y_β} is increasingly negative). This type of behavior is commonly associated with vortical flows, although these flows usually produce forces on the forebody. Addition of the vertical tails generates a positive increment Cn_β values, which results in directional stability up to 10° angle of attack. Between 10° and 18° angle of attack, the vertical tails decrease the stability of the configuration. The flow physics discussed previously concerning the interaction of the wing leading-edge vortex and the vertical tail would also explain these characteristics. Beyond 18° angle of attack, the wing-body directional stability characteristics dominate the configuration and the effect of the vertical tail is minimal.

Figure 22 shows the effectiveness of the tiperons for providing roll control. The tiperons, deflected asymmetrically, generate significant rolling moment increments and the control effectiveness is fairly linear (that is the change in moment versus control deflection is a linear function). Up to 10° angle of attack, the low levels of adverse yawing moment generated by the tiperons is independent of the control deflection angle for deflections above ±12°. Beyond this angle of attack, only the largest deflections increase adverse yawing moments further. In general, the levels of roll control are judged to be adequate, but because of the high levels of static lateral stability, a crosswind analysis must be performed. This analysis will also require the rudder effectiveness data presented in Fig. 23 and will be discussed later in the paper. Like the tiperons, rudder effectiveness is linear with control deflection.

As would be expected, rudder power decreases as angle of attack increases beyond about 8°. This is likely a result of the large wing-body planform shielding the vertical tails and effectively reducing the dynamic pressure at the rudders, although it is possible that a more complex interaction with the wing leading-edge vortex is responsible. Unlike the tiperons, however, the twin rudders produce a favorable cross derivative (rolling moment due to rudder deflection). This means that rudder inputs will tend to be self coordinating, requiring less asymmetric tiperon deflection to make a coordinated turn. This will also have a positive impact on the crosswind capabilities of this configuration.

As mentioned previously, crosswind and coordinated roll analyses were performed. Because approach-to-landing will most likely be the most demanding low-speed flight phase for this vehicle, the conditions chosen for these analyses were as follows: $\alpha = 10°$, V = 151 kts and W = 183,000 lbs. The crosswind analysis simply involves solving a set of simultaneous algebraic equations using the static lateral-directional stability derivatives and the roll and yaw control derivatives. In general, this type of vehicle must demonstrate the ability to land in a 30 kt crosswind. To trim out the sideslip generated by this crosswind and align the vehicle with the runway centerline would require a 24° asymmetric tiperon deflection and a 6° rudder deflection. The rudder requirement is reasonable, using only a small fraction of the available control authority. The tiperon requirement, however, is more severe. When combined with the necessary symmetric tiperon deflection for pitch trim, one of the tiperons will always be deflected to the maximum angle at these conditions, thus reducing nose-down pitch and roll control margins.

While the ability to make a velocity vector roll (or coordinated turn) in this vehicle may not be mandatory, it is desirable and the coordinated turn analysis provides an indication of the relative balance between roll and yaw control. By using the vehicle equations of motion, it is possible to develop a relationship between roll and yaw control so that a turn can be made without generating any sideslip (a coordinated turn). As with the nose-down pitch control analysis presented earlier, this analysis requires values for the moments of inertia of the vehicle. These values have been estimated using the shuttle orbiter (Ref. 14) as a reference point. The orbiter's weight and size are reasonably close to the LoFlyte vehicle's landing configuration. This analysis indicated that for coordinated turns, a 6° rudder deflection would be needed for every 1° of asymmetric tiperon deflection. With a rudder deflection limit of 30°, this would mean that coordinated turns would only be possible for asymmetric tiperon deflections of 5° or less. As a result, if coordinated turns are a requirement for this vehicle then either the configuration will be limited to shallow banked turns or a way to achieve more rudder power must be found.

Alternate Vertical Tail Configurations - In order to address the two directional stability and control problem areas, poor rudder power and directional instability between a = 10° and 18°, alternate locations for the vertical tails were investigated. Four additional geometries were evaluated: 1) using one of the existing vertical tails as a centerline tail; 2) the existing vertical tails mounted 8 inches outboard of the baseline location; 3) the existing vertical tails mounted 4 inches inboard of the baseline location; and 4) the existing vertical tails mounted 4 inches inboard of the characteristics for the first three configurations are compared to the baseline tails in Fig. 24. As can be seen in both the lateral and directional data all three alternate geometries eliminated the adverse interaction between the wing leading-edge vortex and the vertical tails. While the outboard location provided the largest stabilizing increment, the level of directional stability associated with the inboard twin tail location is adequate for this vehicle. The inboard location also allows for the tails to be moved further aft and for the notch in the rudder to be filled in without a physical interference problem between the rudder and the tiperons. Moving the tails aft had only a slight effect on lateral-directional stability, providing a small increase in the level of directional stability. There was, however, a significant increase in the effectiveness of the rudders for the aft tail location. Figure 25 compares the available rudder power for the forward and aft tail positions. Moving the tails aft resulted in close to a 50 percent increase in rudder power. This increase would allow coordinated turns with up to 8° of asymmetric tiperon deflection. While this increase is small, it may make the turning performance of the LoFlyte vehicle more acceptable.

Concluding Remarks

Both wind tunnel tests achieved the objectives of creating a data base for subsonic aerodynamic characteristics of waverider-derived configurations.

The aerodynamic characteristics of the integrated vehicles were evaluated and the effectiveness of control surfaces for pitch control and trim as well as lateral/directional stability were examined. Flow visualization data were used to determine leading edge vortex location. This information will help to relocate surfaces in future designs that may result in more favorable characteristics. The aerodynamic characteristics of the two models were similar in several respects. The maximum L/D values observed for each configuration were comparable. Both models exhibited neutral or unstable pitching moment characteristics at the conditions studied. The tiperons on Model 2 were observed to be more effective than the elevons on Model 1 for pitch control. Both configurations exhibited stable lateral-directional characteristics of similar magnitudes.

The aerodynamic characteristics of two Mach 4.0 waverider-derived hypersonic cruise configurations were shown for freestream dynamic pressures of 85 and 90 psf. An analysis of the aerodynamic characteristics of the two configurations showed that the cranked-wing design offered only a slight advantage in subsonic aerodynamic performance over the conventional straight-wing design. The straight-wing configuration may provide better vehicle integration characteristics than the cranked-wing design and therefore, may be the preferred design for a hypersonic cruise mission. Both configurations are longitudinally unstable at the conditions studied. The longitudinal stability may be improved by shifting the center of gravity forward through fuel placement or vehicle packaging. Both configurations have good lateral-directional stability characteristics, with the fixed vertical tail contributing significantly to directional stability. The ailerons were observed to be more effective in pitch control than the elevons at low angles of attack. The roll control effectiveness of the ailerons and the effects of combined roll and pitch control for the straight-wing configuration were also presented. The only significant difference in control effects between the straight-wing and cranked-wing vehicles was that the cranked-wing ailerons were significantly less effective in roll control than the straight-wing ailerons and produced significantly more adverse yaw at comparable conditions.

In general, the low speed characteristics of the LoFlyte model are satisfactory. Because of the pitching moment characteristics of this configuration (neutral-to-unstable static margin and positive $C_{m,o}$) the vehicle has a reasonably high level of unpowered trimmed C_L at nominal takeoff and approach-to-landing conditions. This should allow for acceptable takeoff and landing speeds for this vehicle. Locating the vertical tails inboard of the baseline location improved a directional stability problem between 10° and 18° angle of attack. Lateral-directional stability and control characteristics are such that crosswind and coordinated turn criteria can be met although control saturation remains an issue in both cases. Reduction in static lateral stability or a modified approach-to-landing profile would alleviate the control saturation problem during crosswind landings. Higher levels of yaw control are necessary to address this issue for coordinated turns. Moving the vertical tails inboard and aft of the baseline location does improve rudder power, however, the increase in the coordinated turn envelope is small.

Acknowledgement

The authors would like to thank Robert M. Pap of the Accurate Automation Corporation for providing the LoFlyte wind tunnel model used to generate data for this paper.

References

1. Pegg, R. J. et al: Design of a Hypersonic Waverider-Derived Airplane. AIAA Paper 93-0401, 1993.

2. Townend, L. H.: Research and Design for Lifting Reentry. Progress, in *Aerospace Sci.*, Vol. 18, 1979, pp. 1–80.

3. Bowcutt, K. G.; Anderson, J. D.: Viscous Optimized Hypersonic Waveriders. AIAA 87-0272, 1987.

4. Anderson, J. D.; Lewis, M.; and Corda, S.: Several Families of Viscous Optimized Waveriders—A Review of Waverider Research at the University of Maryland. Proceedings of 1st International Hypersonic Waverider Symposium, October 1990.

5. O'Neill; Lockwood, M. K.: Design Tradeoffs on Scramjet Engine Integrated Hypersonic Waverider Vehicles. *Journal of Aircraft*, Vol. 30, No. 6, Nov.–Dec. 1993, pp. 943–952.

Table 2. Model 2: 12-Foot Low-Speed Tunnel

qbar = 4 psf		α1	2,14,16,18,20	
		β1	2,0,2,4,6,8,10	
		delta tiperon	delta rudder	
α	β	left/right	left/right	Comments
α1	0,-4,4	0/0	0/0	Tails on; engine off
0,8,12,20	β1	0/0	0/0	
α1	0,-4,4	0/0	OFF	Engine/tails off
0,8,12,20	β1	0/0	OFF	
α1	0,-4,4	0/0	OFF	Engine on; tails off
0,8,12,20	β1	0/0	OFF	
α1	0,-4,4	0/0	0/0	Full configuration
-4,0,4,8,12,16,20	β1	0/0	0/0	
α1	0,-4,4	10/10	0/0	Pitch Control
α1	0,-4,4	20/20	0/0	
α1	0,-4,4	30/30	0/0	
0,8,12,20	β1	30/30	0/0	
α1	0,-4,4	-30/-30	0/0	
0,8,12,20	β1	-30/-30	0/0	
α1	0,-4,4	-20/-20	0/0	
α1	0,-4,4	-10/-10	0/0	
α1	0,-4,4	-30/-10	0/0	Combined Roll/Pitch Control
0,8,12,20	β1	-30/-10	0/0	
α1	0,-4,4	-30/10	0/0	
0,8,12,20	β1	-30/10	0/0	
α1	0,-4,4	-30/-30	Off	
0,8,12,20	β1	-20/-10	0/0	
α1	0	-20/10	0/0	
8,12	β1	-20/10	0/0	
α1	0	20/10	0/0	
8,12	β1	20/10	0/0	
α1	0	20/-10	0/0	
8,12	β1	20/-10	0/0	
α1	0,-4,4	30/-10	0/0	
0,8,12,20	β1	30/-10	0/0	
α1	0,-4,4	30/10	0/0	
0,8,12,20	β1	30/10	0/0	
α1	0	0/0	10/10	Yaw Control
8,12	β1	0/0	10/10	
α1	0	0/0	20/20	
8,12	β1	0/0	20/20	
α1	0	0/0	30/30	
0,8,12,20	β1	0/0	30/30	
α1	0	-30/0	0/0	Roll Control
α1	0	-20/0	0/0	
α1	0	-10/0	0/0	
α1	0	10/0	0/0	
α1	0	20/0	0/0	
α1	0	30/0	0/0	
α1	0,-4,4	0/0	0/0	Tails moved 8" outboard from baseline
0,8,12,20	β1	0/0	0/0	
α1	0	0/0	10/10	
α1	0	0/0	20/20	
α1	0	0/0	30/30	
α1	0	0/0	30/30	Tails 8" outboard; rudder notch filled
α1	0,-4,4	0/0	0	Centerline Tail
α1	0	0/0	30	
α1	0,-4,4	0/0	0/0	Tails moved 4" inboard from baseline
α1	0	0/0	10/10	
α1	0	0/0	20/20	
α1	0	0/0	30/30	
α1	0,-4,4	OFF	OFF	Wing tips/tails off; engine on
0,8,12,20	β1	OFF	OFF	
α1	0	0/0	10/10	Tails moved 4" IB; Rudder HL at wing TE; w/
α1	0	0/0	20/20	Rudder notch filled
α1	0	0/0	30/30	
α1	0,-4,4	0/0	0/0	

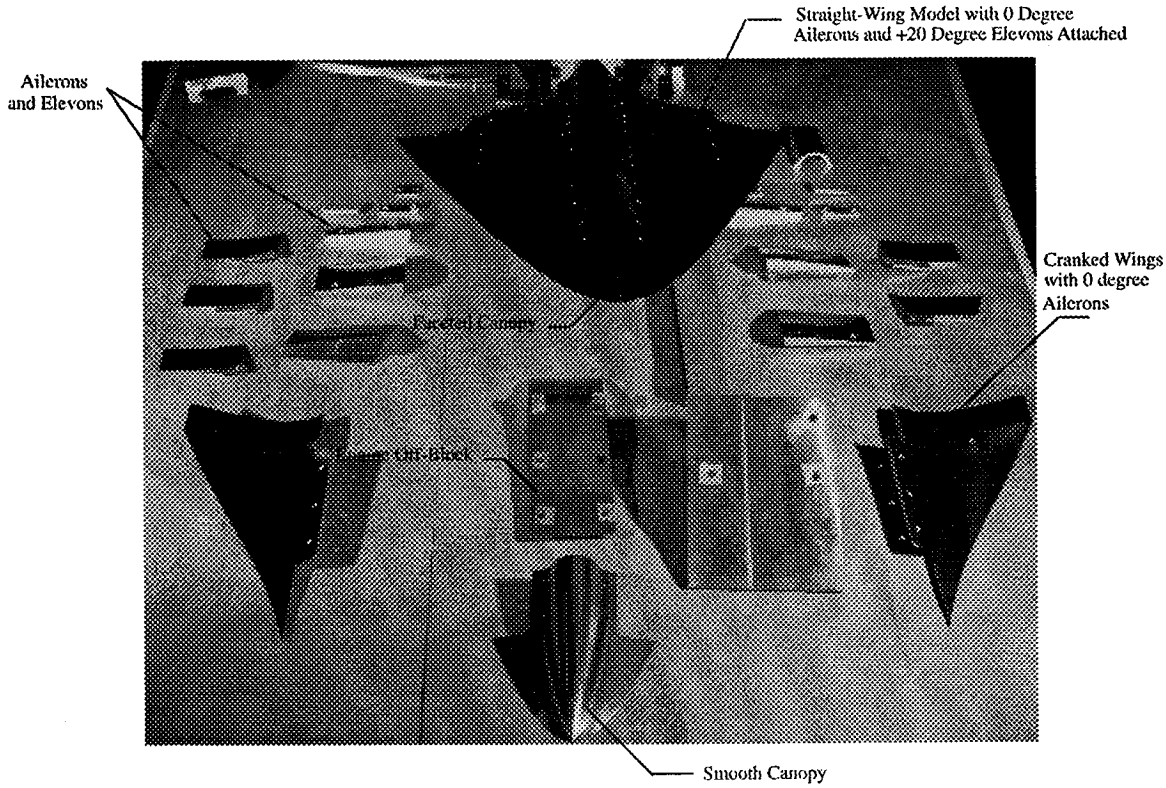

Fig. 1. Photograph of Mach 4 waverider-derived wind-tunnel model with various vehicle components.

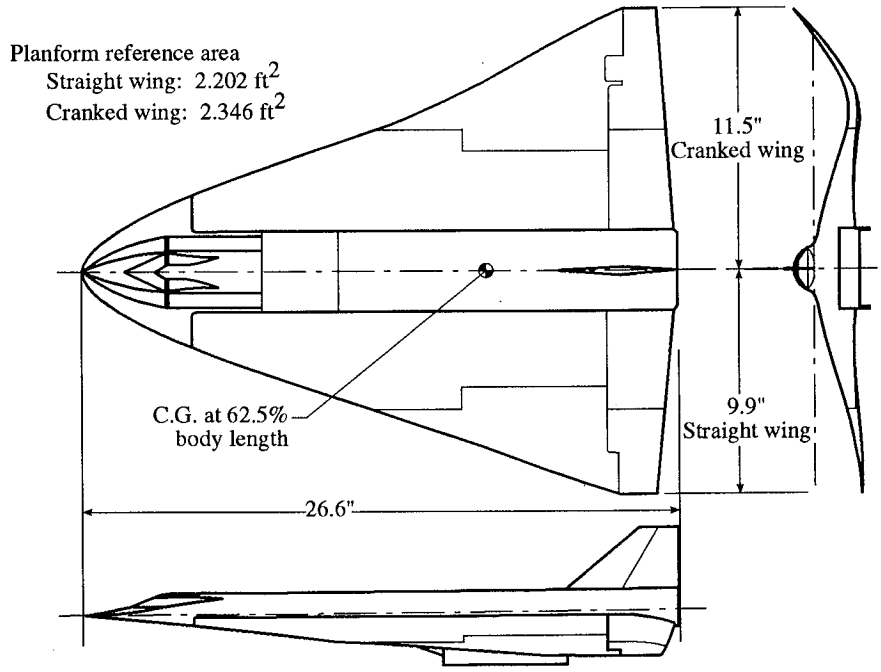

Fig. 2. Mach 4 waverider-derived hypersonic cruise configuration.

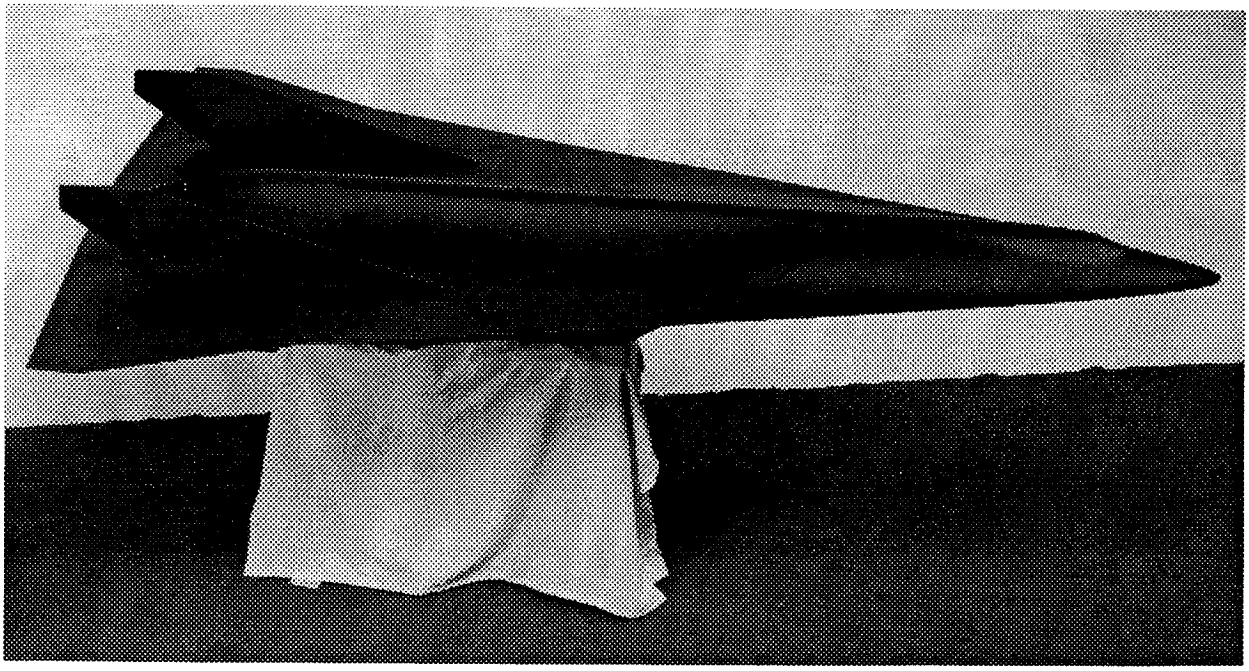

Fig. 3. Photograph of .062 scale wind tunnel model of LoFlyte.

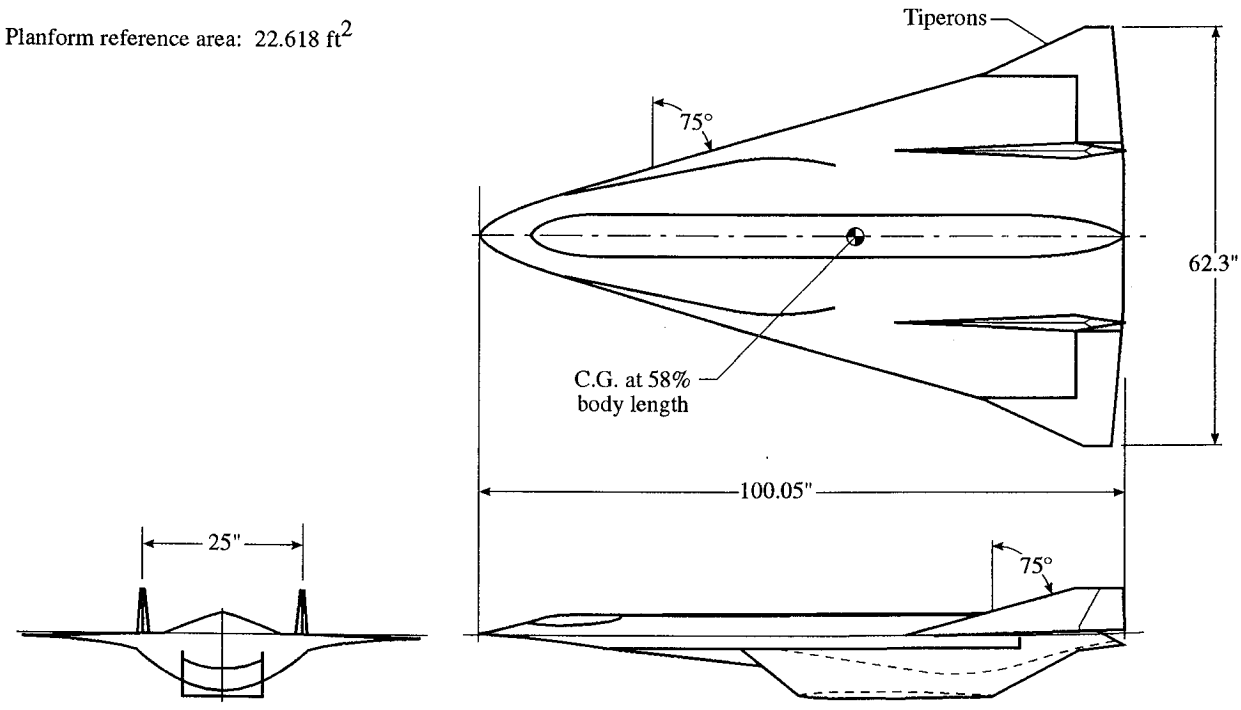

Fig. 4. Mach 5 optimized hypersonic vehicle, LoFlyte.

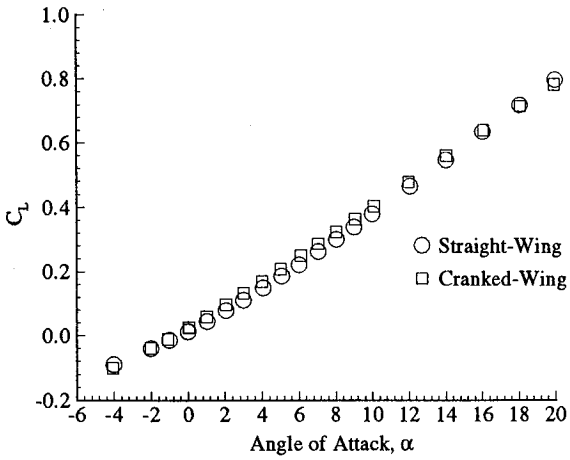

Fig. 5. Comparison of lift coefficient values for straight wing and cranked-wing waverider vehicles.

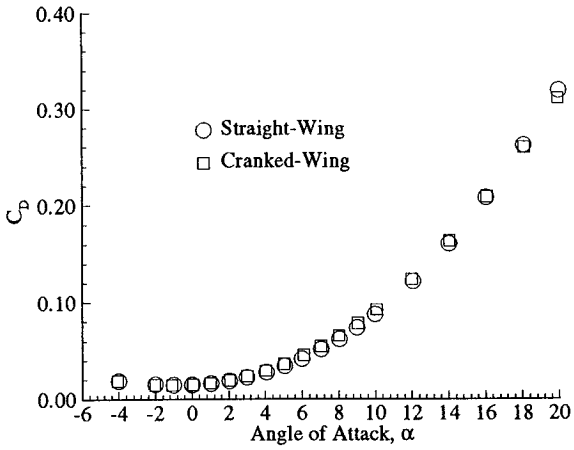

Fig. 6. Comparison of drag coefficient values for straight-wing and cranked-wing waverider vehicles.

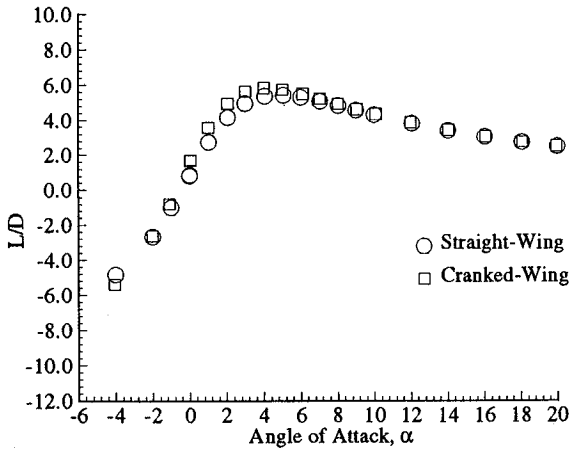

Fig. 7. Comparison of lift-to-drag ratios for straight wing and cranked-wing waverider vehicles.

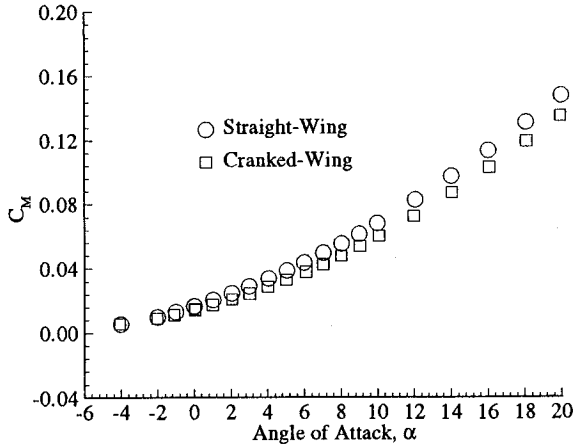

Fig. 8. Comparison of pitching moment data for straight-wing and cranked-wing waveriders.

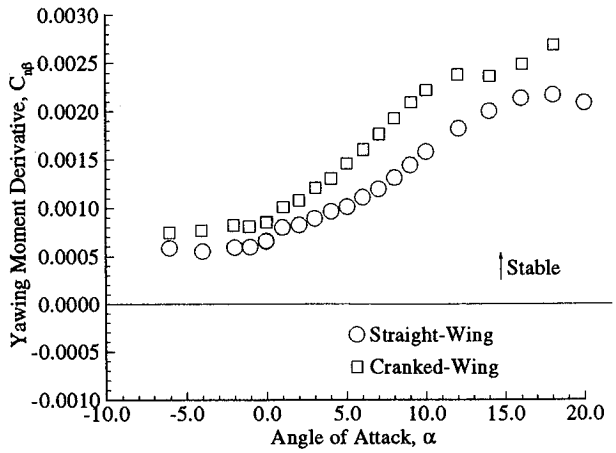

Fig. 9. Directional stability of straight-wing and cranked wing waverider vehicles.

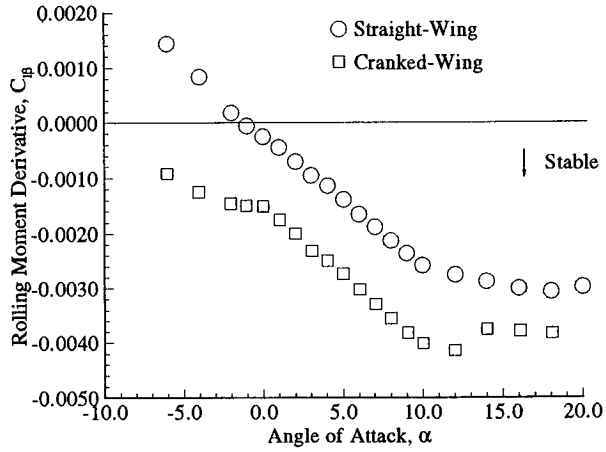

Fig. 10. Lateral stability of straight-wing and cranked-wing waverider vehicles.

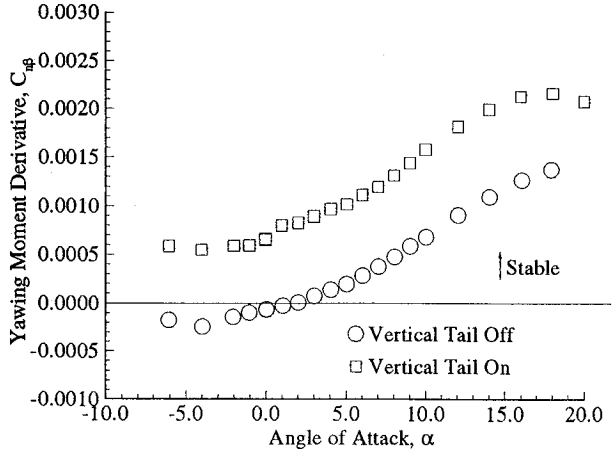

Fig. 11. Effect of vertical tail on directional stability of straight-wing waverider model.

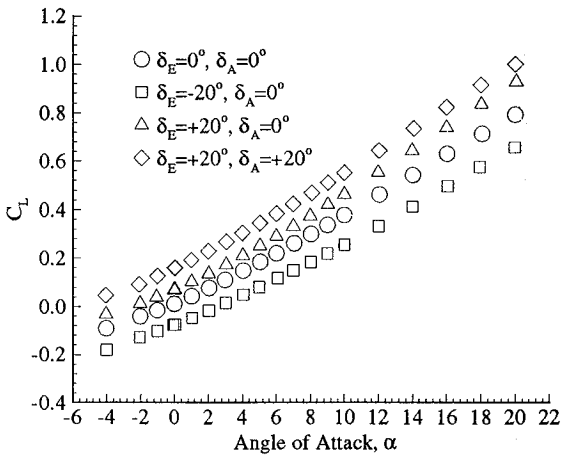

Fig. 12. Effect on lift coefficient of straight-wing control surface deflections.

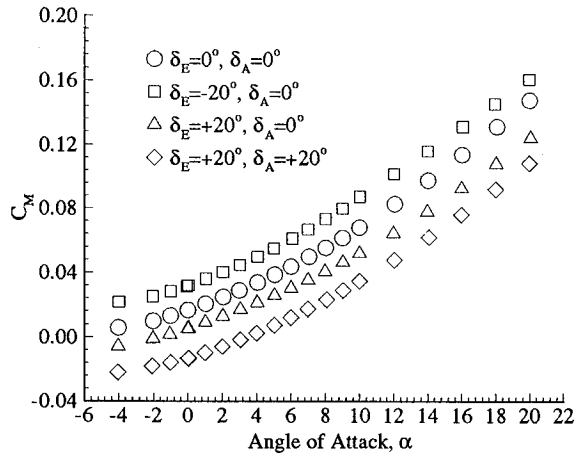

Fig. 13. Effect on pitching moment of straight-wing control surface deflections.

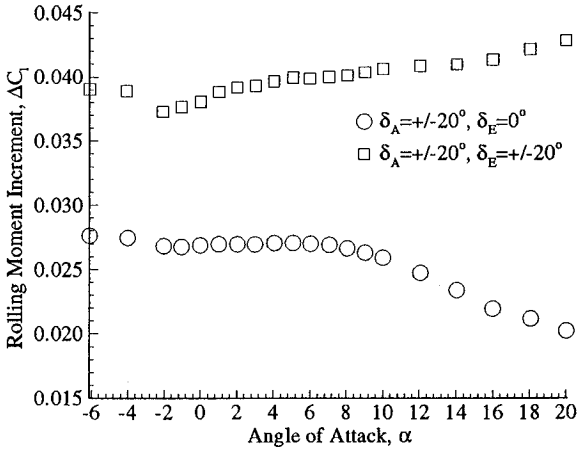

Fig. 14. Rolling moment increments produced by straight-wing control surfaces.

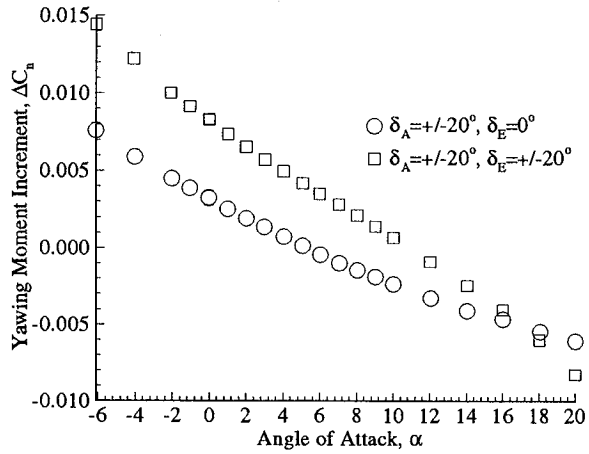

Fig. 15. Yawing moment increments produced by straight-wing control surfaces.

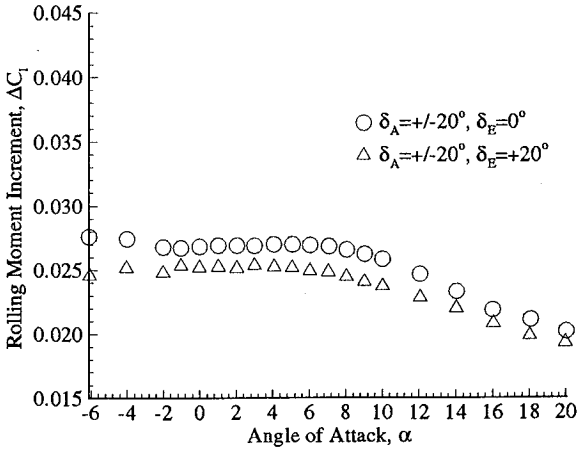

Fig. 16. Rolling moment increments produced by combined roll-pitch deflections.

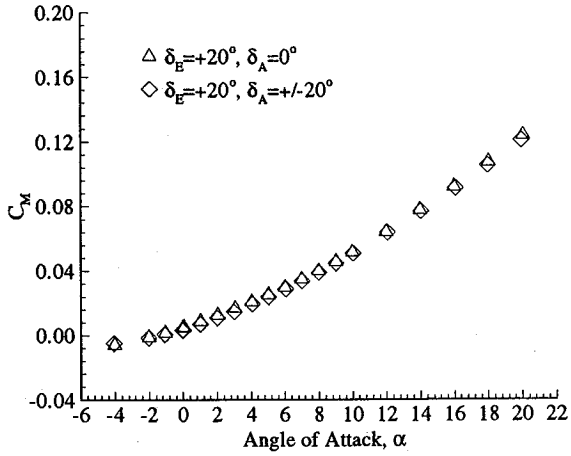

Fig. 17. Effect of combined roll/pitch control on pitching moment coefficients.

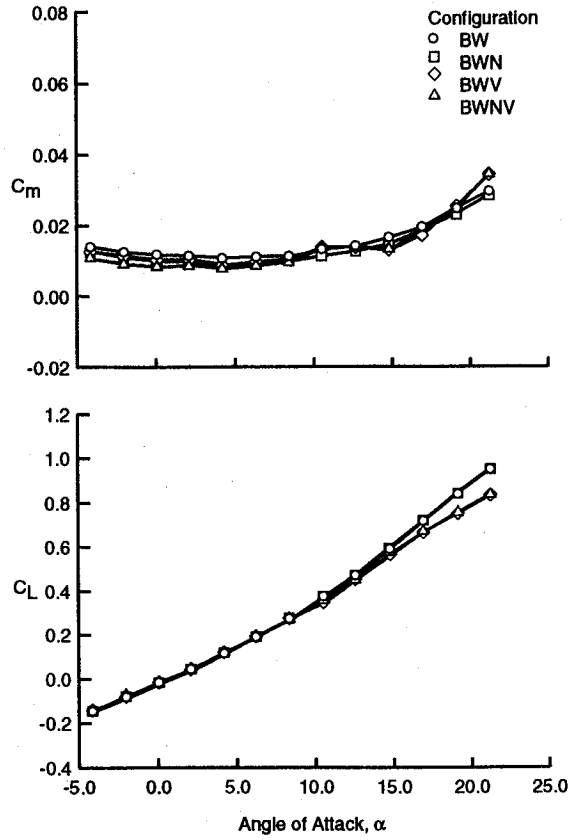

Fig. 18. Configuration build-up.

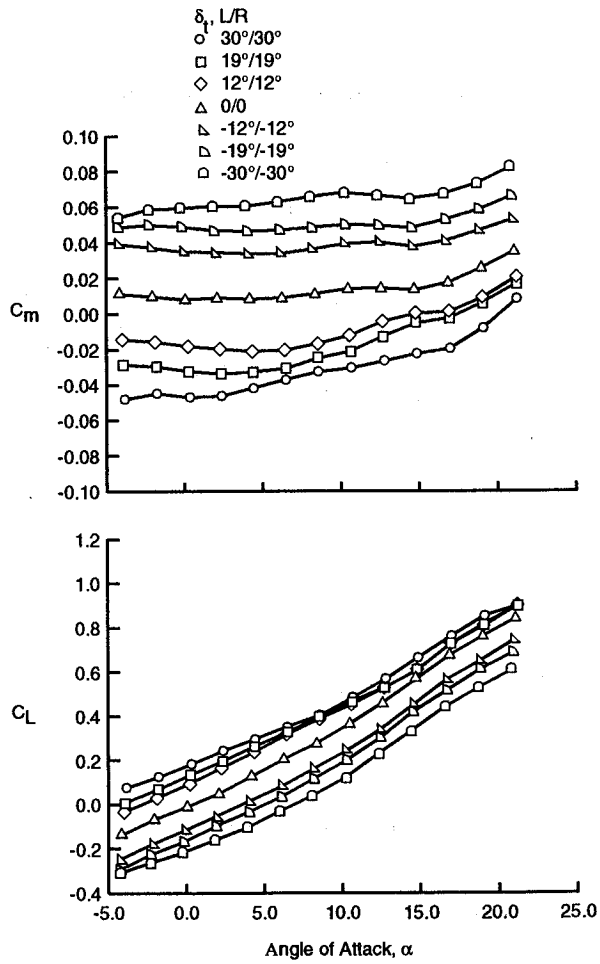

Fig. 19. Effect of tiperons for pitch control.

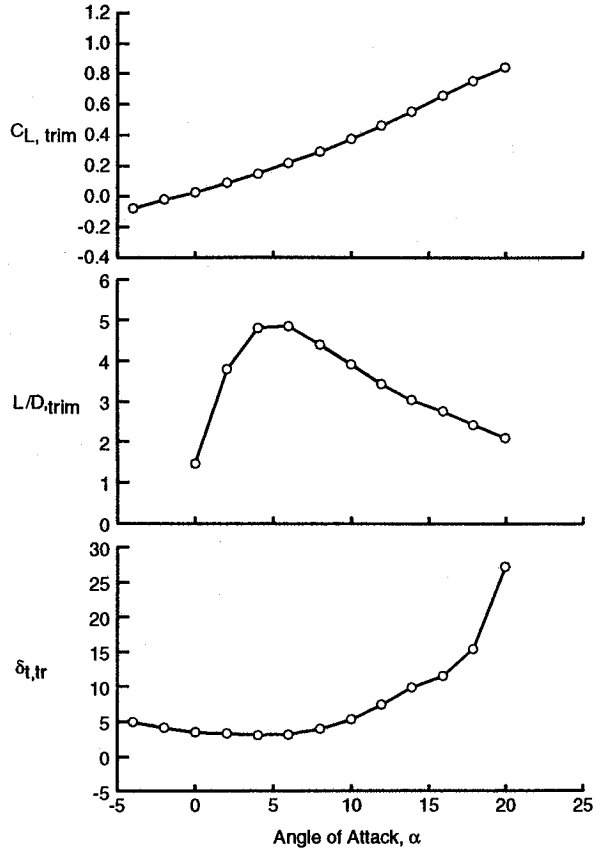

Fig. 20. Trimmed longitudinal characteristics.

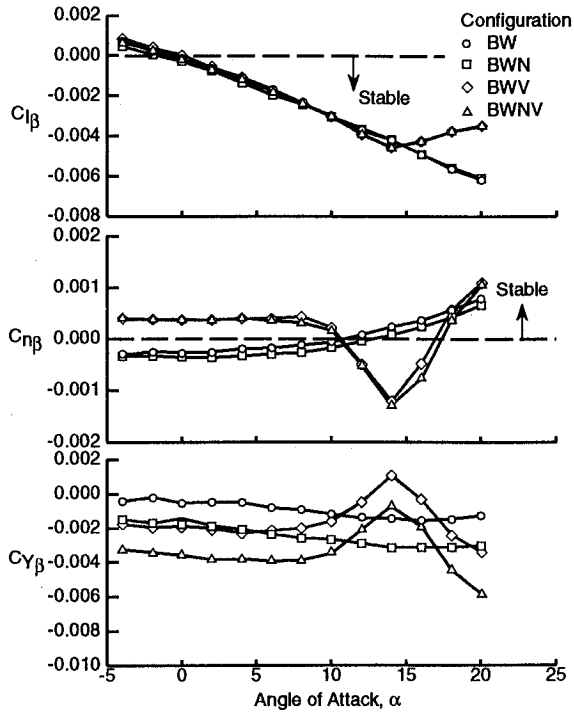

Fig. 21. Effect of configuration build-up on the lateral/directional stability characteristics.

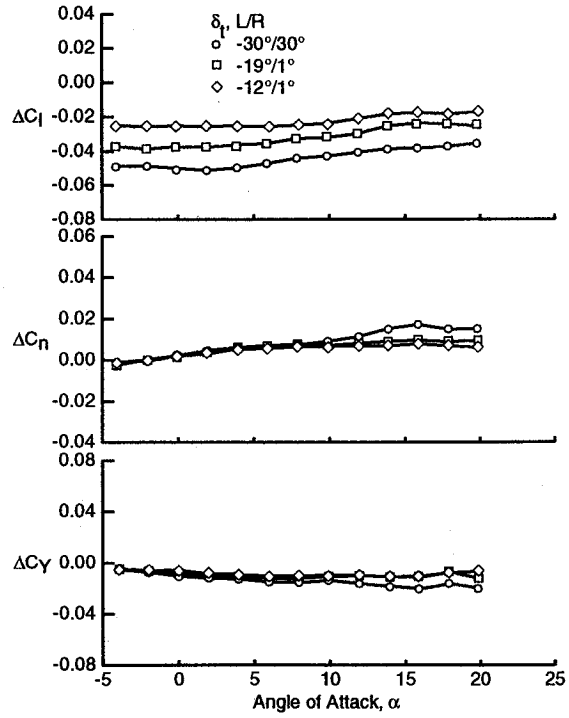

Fig. 22. Effect of tiperons for roll control.

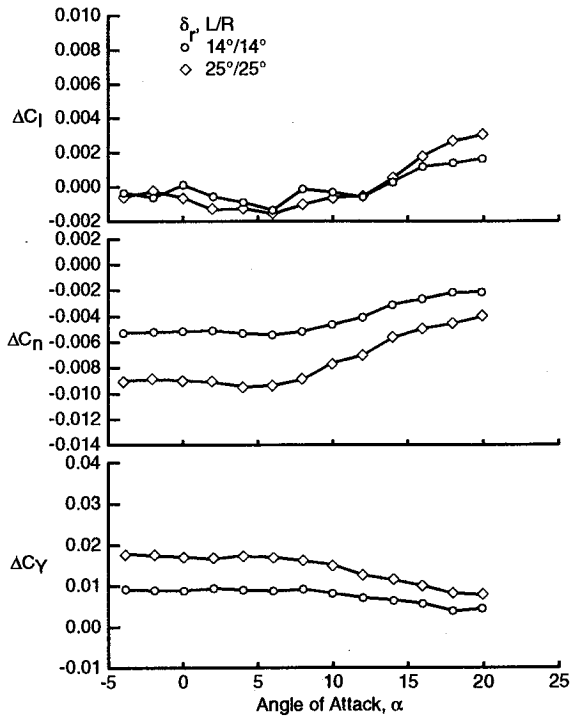

Fig. 23. Rudder effectiveness.

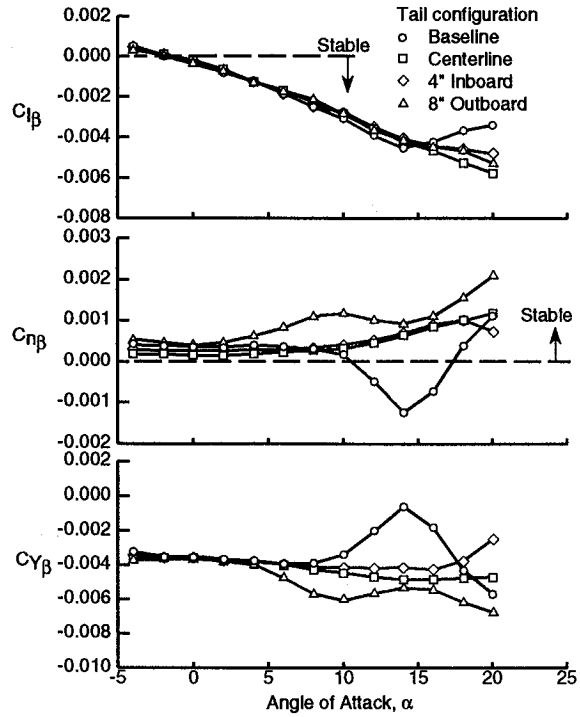

Fig. 24. Effect of vertical tail location on the lateral/ directional stability characteristics.

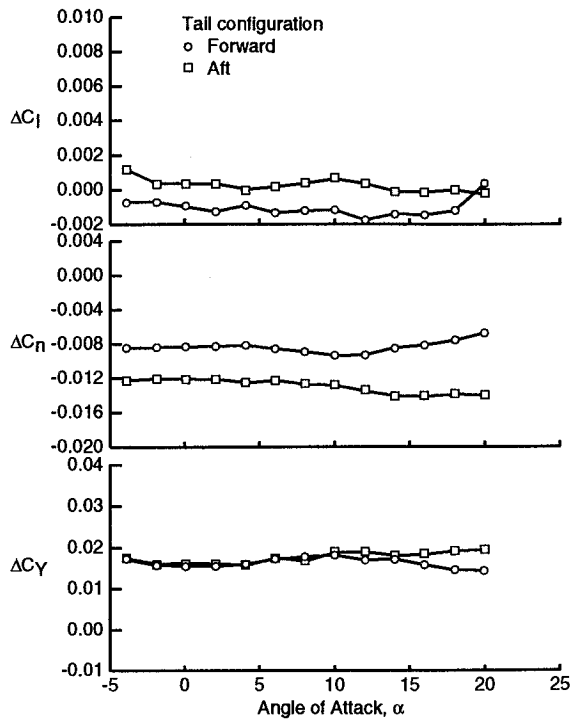

Fig. 25. Effect of longitudional tail position on rudder power. Vertical tail 4" inboard; rudder = 25°/25°